International Journal of Greenhouse Gas Control 125 (2023) 103888

Contents lists available at ScienceDirect

International Journal of Greenhouse Gas Control

journal homepage: www.elsevier.com/locate/ijggc

Improvement in CO_2 geo-sequestration in saline aquifers by viscosification: From molecular scale to core scale

Salar Afra [a], Mohamed Alhosani [b], Abbas Firoozabadi [a,b,*]

[a] Reservoir Engineering Research Institute, 595 Lytton Avenue, Suite B, Palo Alto, CA 94301, United States
[b] Chemical and Biomolecular Engineering Department, Rice University, Houston, TX 77005, United States

ARTICLE INFO

Keywords:
CO_2 viscosification by an oligomer of 1-decene
Residual brine saturation
CO_2 brine saturation reduction
CO_2 sequestration

ABSTRACT

Carbon dioxide (CO_2) storage in the subsurface is a viable approach to mitigate climate change by reducing anthropogenic greenhouse gas emissions. The unfavorable mobility ratio in brine displacement by CO_2 would lead to poor sweep efficiency. In this investigation, the efficiency of an engineered CO_2 oligomer viscosifier with about twenty repeat units of 1-decene is evaluated in mobility control and sweep efficiency improvement in drainage. We have performed brine displacement experiments in sandstone rock with supercritical CO_2. The viscosifier at 1.5 wt% concentration increases the viscosity of supercritical CO_2 by 4.8 folds at pressure of 3500 psi and temperature of 194 ℉. We observe significant delay of CO_2 breakthrough time by 2.6 ± 0.1 folds in a large number of experiments by viscosified CO_2. The molecule does not have appreciable adsorption on the rock surface. The pressure drop from displacement of neat CO_2 by viscosified CO_2 at 1 PV injection provides the evidence of low adsorption. Molecular simulations are conducted to investigate adsorption. Low adsorption is a key measure of the effectiveness of the molecule. The results from molecular simulations agree with the experiments. In addition to viscosification, the novelty of the molecule is that there is a significant decrease in the residual brine saturation. Consequently, the residual trapping is also increased. The combination of decrease in residual brine saturation, and mobility control are expected to significantly improve the storage capacity through increase in residual trapping and sweep efficiency in CO_2 storage in saline aquifers. As a result, CO_2 storage may become more efficient.

1. Introduction

The atmospheric concentration of carbon dioxide (CO_2), as the most abundant greenhouse gas (GHG), has been rising rapidly since the Industrial Revolution from 280 ppm to about 420 ppm in 2020. The rate of increase in CO_2 concentration has risen from 1 ppm per year in 1960 to 2.4 ppm per year in 2020 (Letcher, 2021). Carbon capture and storage (CCS) is among the most cost-effective pathways to control and mitigate CO_2 contribution in climate change (Aminu et al., 2017). The geological formations in which CO_2 could be sequestered and stored include coal-bed methane formations (Mukherjee and Misra, 2018), shale formations undergoing CO_2-based enhanced oil recovery (EOR) (Kolster et al., 2017), saline aquifers (Kim et al., 2017), and depleted oil and gas reservoirs (Tayari and Blumsack, 2020). Saline aquifers seem to be the most promising option due to distinct features in formations which have high permeability, high porosity, and very large sizes that provide a substantial potential storage capacity (400 to 10,000 Gt of CO_2) (Aminu et al., 2017).

CO_2 is typically in a supercritical state in aquifers; it may migrate upward as a plume due to the buoyancy until reaching the caprock. The storage from continuous CO_2 saturation close to the caprock is referred to as structural trapping (Iglauer et al., 2015), which is the least reliable storage from safety considerations since CO_2 remains mobile (MacMinn et al., 2010). In displacement and in upward movement of the plume, part of the CO_2 would trap in the formation pores as ganglia through capillary forces. The trapping mechanism is referred to as residual trapping (Pentland et al., 2011). Part of CO_2 would dissolve in the brine, which often results in a density increase of about 1 wt% depending on pressure and temperature. The density increase will put in motion the transfer of CO_2 downward to the bottom of the formation when permeability is high (Mutoru et al., 2011; Ennis-King et al., 2005). The immobilization of CO_2 through dissolution in brine, which is referred to as solubility trapping, is the safest and most desirable trapping mechanism. CO_2 in contact with brine may also react with the rock minerals

* Corresponding author at: Reservoir Engineering Research Institute, 595 Lytton Avenue, Suite B, Palo Alto, CA 94301, United States.
E-mail address: abbas.firoozabadi@rice.edu (A. Firoozabadi).

https://doi.org/10.1016/j.ijggc.2023.103888
Received 3 June 2022; Received in revised form 3 April 2023; Accepted 10 April 2023

and immobilize from precipitation. The mineralization is considered to be very secure, but it is slow and deemed to be a long-term trapping mechanism (Gershenzon et al., 2014).

To improve the efficiency of CO_2 sequestration, it is desirable to control its mobility. The processes include implementing water-alternating-gas (WAG) injection, CO_2-direct viscosification, and the formation of CO_2-in-brine foam. Among these options, CO_2 direct viscosification is the most desirable because water injection is not required, control of the process is practical, and it obviates concerns such as corrosion (Heller et al., 1985). In addition to mobility decrease of CO_2, reduction of residual brine from CO_2 displacement will also add to efficiency of CO_2 sequestration. There is additional benefit from residual brine saturation decrease. It promotes CO_2 dissolution.

Application of foam to improve CO_2 storage capacity and enhance capillary trapping in saline aquifers has been reported in different studies (Føyen et al., 2020; Alcorn et al., 2020; Adebayo, 2018). Formation of strong foam has been also discussed using different types of non-ionic and ionic surfactants in a long vertical sandstone core (Føyen et al., 2020). In a sandstone, there is report of decrease in residual water saturation from 0.34 (in neat CO_2) to 0.16 in CO_2-foam at pressure of 2900 psi, temperature of 104 to 176 ℉, and brine salinity of 3.8 wt%. Nanoparticle-CO_2 foam effect on CO_2 mobility at pore (etched silicon wafer micromodel) and core (high permeability, 1400 mD, horizontal Bentheimer sandstone) have been also reported at pressure of 2900 psi, temperature of 104 ℉, and 35,000 ppm NaCl brine (Alcorn et al., 2020). Despite advances in CO_2-foam mobility control, there are issues from foam stability during prolong injection and significant decrease in injectivity. CO_2 direct viscosification is an alternative to foam with various advantages (Heller et al., 1985). The main challenges in CO_2 direct viscosification have been in finding CO_2 soluble molecules that can adequately increases CO_2 viscosity and maintain solubility and viscosity at aquifer conditions. The molecule should not adsorb onto the rock surface (Lemaire et al., 2021). Solubility in CO_2 and viscosification of different molecules have been studied experimentally and by molecular simulations (Enick et al., 2012; Goicochea and Firoozabadi, 2019).

Coreflooding in which brine is displaced by neat and viscosified CO_2 and comparison of performance is the clear path in evaluation (Sun et al., 2016). The results from core flooding can be used in simulation of flow path and plume migration at field scale (Kumar et al., 2004; Celia et al., 2015). There are a large number of publications on CO_2 injection in brine-saturated sandstone and carbonate cores (Müller, 2011; Mathias et al., 2013). To the best of our knowledge, there is one report of viscosified CO_2 injection in brine displacement in core flooding experiment (Zaberi et al., 2020). The study reports displacement of 38.3% PV of water from an initially brine-saturated core by neat CO_2 injection. The subsequent injection of viscosified CO_2 (1 wt% polyfluoroacrylate (PFA)) yielded an incremental 2.5% PV extra brine. However, due to strong adsorption of PFA to the rock surface, the effective permeability to CO_2 decreases by 30 times (from 7.3 mD to 0.25 mD) for a limited pore volume injection. (This study also presented results for brine recovery from dual parallel sandstone cores.)

In this work, the focus is on brine displacement in sandstone rocks. In addition to brine displacement, we also investigate adsorption by molecular simulations, and displacement of neat CO_2 by viscosified CO_2 in coreflood experiments. In molecular simulations, we select three types of CO_2-viscosifying polymers that represent most of the work in the literature on viscosification of CO_2. Molecular simulations show that two of the three molecules adsorb strongly onto calcite and quartz. Another molecule is selected to represent oligomers of 1-decene with six repeat units. In the experiments, the cores are placed horizontally to investigate the effect of viscosification by brine displacement in most cases. We also conduct two experiments with cores in vertical orientation. These displacements provide insight on residual brine saturation in neat and viscosified CO_2 injection experiments. We present the successful application of CO_2 viscosification in enhancing brine displacement through mobility control and decrease of residual brine saturation. The decrease in mobility and residual brine saturation lead to significant improvement in capacity and security of stored CO_2 in saline aquifers.

2. Materials and methods

2.1. Materials

Poly-1-decene (P1D) samples with an average molecular weight of 910 g/mol (Sigma-Aldrich), and 2950 g/mol (Kar and Firoozabadi, 2022) synthesized by Lubrizol) are used in this work. The data for viscosity of the two polymers are: 42 cp at 40 °C (Sigma Aldrich website), and 55 cp at 100 °C (provided by Lubrizol), respectively. Polydispersity index (PDI) data for these two polymers are not available. The molecular weights are determined by the suppliers.

Potassium chloride (Fisher Chemical, certified ACS), sodium chloride (Sigma-Aldrich, 99.5%), strontium chloride (Acros, 99%), magnesium chloride (Sigma-Aldrich), and deionized water are used to prepare brine solutions at salt concentrations of 50 and 73 g/L. The effect of salinity on performance of the P1D with an average molecular weight of 2950 g/mole is part of this investigation. Two different homogenous (based on the information provided by Kocurek Industries, Inc., and CT scans) sandstone rock samples, high and intermediate permeability, are used in this study. Core flooding experiments are conducted in two core lengths, 10 and 24 inches to examine capillary end effect. The relevant data are presented in Table 1.

2.2. Viscosity measurement

Published data on viscosity of thickened CO_2 for P1D with six repeat units vary widely by various authors; with reports of viscosity increases ranging from greater than order-of-magnitude at 0.5wt% oligomer to only a few percent at 2 wt% oligomer. One reason for a large disparity may be due to ineffective mixing of the polymer and CO_2 that often leads to lower viscosification. Viscosity measurements and deposition of the polymer within the viscometer may be also another source of the problem because small undissolved droplets or particles would lead to erroneously high values of viscosity readings via partially clogging a capillary or impeding the movement of a falling or rolling object. Kar and Firoozabadi (2022) discuss in detail viscosity measurements for P1D with an average molecular weight of 910 g/mol (six monomers). We have designed and assembled an in-house-built setup for conducting mixing. The mixing setup (accumulator), and viscosity measurements are presented in the supporting information (neither the viscometer nor the mixer are windowed).

2.3. Coreflood experiments

Coreflood experiments are conducted using an in-house designed and assembled system which is discussed in the supporting information. The coreflood experiments are intended at field conditions of CO_2 storage in a large saline aquifer in Europe. All the experiments except two are conducted in horizontal cores. Two experiments are conducted in vertical cores to measure residual brine saturation. We do not saturate brine with CO_2 to have conditions similar to the field. CO_2 is in a supercritical state in our core flooding experiments. The pressure and temperature in our core flooding experiments are based on field conditions. As a whole, in CO_2 subsurface sequestration, the conditions are selected for high CO_2 density.

3. Molecular simulations

In our adsorption investigation, we select three group of molecules which have shown promise in CO_2 viscosification. Fluorinated molecules are by far the most widely studied and effective. However, they are

Table 1
Experimental conditions and rock propertied and dimensions in the coreflood experiments.

Category	Test #	Permeability (mD)	Porosity (%)	Length (inch)	Temperature (F)	Salinity (g/L)	Salt
Adsorption Evaluation	1	720	21	10	194	–	
	2	97	22	10	194	–	
	3	90	22	10	194	–	
Brine displacement (Short Cores)	4	655*	20	10	194	50	KCl
	5	655*	20	10	194	50	KCl
	6	665**	21	10	158	50	KCl
	7	665**	21	10	158	50	KCl
	8	87	22	10	194	73	Mixture***
	9	95	21	10	194	73	Mixture***
	10	91	22	10	194	50	NaCl
	11	85	23	10	194	50	NaCl
Brine displacement (Long Cores)	12	510	23	24	194	73	NaCl
	13	525	23	24	194	73	NaCl
	14	473	23	24	194	73	NaCl
	15	492	23	24	194	73	NaCl
Brine displacement (Vertical Short Cores)	16	83	23	10	194	73	NaCl
	17	90	23	10	194	73	NaCl

Core diameter =1.5 inches. Pore pressure =3500 psi.
* Same core used in Tests 4 and 5.
** Same core used in Tests 6 and 7.
*** Na 12 g/L, Ca 5 g/L, Mg 5 g/L, Sr 2.5 g/L, and K 2.5 g/L.

expensive and environmentally undesirable. Polymers of 1-decne (P1D) with an average molecular weight of 910 g/mol (six repeat units) have been studied extensively in the past; it has mild effectiveness (Heller et al., 1985; Zhang et al., 2011; Al Hinai et al., 2017). We use the oligomer of 1-decene with about 20 repeat units which is much more effective than the six-repeat unit of 1-decne (Kar and Firoozabadi, 2022). The third molecule is an effective new co-polymer (Zhang et al., 2021). We have selected the molecule among a group which shows the most effectiveness (Zhang et al., 2021); it is based on epoxide heptamethyltrisiloxane and glycidyl phenyl ether (EHGP). In this work we refer to it as the EHGP co-polymer. We use Steered Molecular Dynamics (SMD) simulations to investigate adsorption at 185 F and 7700 psi. The adsorption of P1D with six repeat units, an effective fluorinated co-polymer, polyheptadecafluorodecyl acrylate polymerized with styrene (HFDA) from Huang et al. (2000), and the co-polymer from Zhang et al. (2021) are investigated onto calcite and α-quartz surfaces. These three molecules represent viscosifiers that viscosify CO_2 by various degrees. In our molecular simulations we use part of the true HFDA. We also use a polymer of P1D with six monomers which is smaller than the oligomer of 1-decene with about twenty repeat units (average molecular weight of 2950 g/mol). If part of HFDA, and P1D with six monomers adsorb, the full molecule of HFDA and P1D with higher number of repeat units may also adsorb.

In the past, we have used SMD simulation to investigate adsorption of various polymeric surfactants on hydrate surfaces (Jiménez-Ángeles and Firoozabadi, 2018). There is agreement with the experimental data. Briefly, in the SMD simulations, a reaction coordinate is selected to indicate the position of the target molecule during the movement for studying the variation of free energy. The free energy change (ΔG), that is the potential of mean force is plotted vs. the reaction coordinates. The SMD simulations, in principle, are directly comparable to AFM-FS experiments when the same bond loading rates are applied (Titiloye et al., 1998).

3.1. Molecular model

All systems are built using the MedeA software's amorphous builder (see France-Lanord et al. (2014)). Two solid substrates (calcite and α-quartz) are built with different dimensions, each using six atomic layers along the *z*-direction, which is the direction normal to the [1014] surface for calcite and the [101] surface for α-quartz. These two surfaces are considered to be the most stable (Titiloye et al., 1998; De Leeuw and Parker, 1998; De Leeuw, 2002; Koleini et al., 2019; Sedghi et al., 2016; Wright and Walsh, 2012; Wu et al., 2013). The P1D and HFDA viscosifiers are modeled following the descriptions by Goicochea and Firoozabadi (2019), Gama Goicochea and Firoozabadi (2019). Fig. 1 depicts the molecular structures of the three CO_2 viscosifiers. To construct the initial configuration, a CO_2 fluid phase is placed between two solid substrates, creating a sandwiched system along the *z*-direction, and the viscosifier molecule is then placed at the center of the CO_2 phase, approximately 3 nm away from the two surfaces for the three polymers (Fig. 2). We use 5300 CO_2 molecules in our simulations.

3.2. Simulation procedure

All simulations are performed at 185 F and 7700 psi using the LAMMPS (Plimpton, 1995) code integrated in the MedeA software environment. We have selected the pressure and temperature conditions at which there are data for all the three molecules. The bonded and nonbonded energies for all the molecules are described by the all-atom force field PCFF+ (an extension of the PCFF force field) (Yiannourakou et al., 2013). The force field accurately reproduces the thermodynamic properties of organic compounds as well as the structure of organic molecules and polymers. A number of studies have reported validation of the force field against experimental data (Ungerer et al., 2015; Collell et al., 2014; Ungerer et al., 2014). The long-range electrostatic interactions are described using the particle-particle-particle-mesh (PPPM) method, with an accuracy criterion of 0.001% for the grid size (Eastwood et al., 1980). The cutoff distances for the nonbonded interactions and the pair interactions are the same in PCFF+, and a value of 12 Å is used for both. The sixth power-mixing rules by Waldman and Hagler (1993) are employed for the unlike atoms. The equations of motion are integrated at a time step of 1 fs. The temperature and pressure are controlled using a Nose-Hoover thermostat (Hoover, 1985) and barostat (Hoover, 1986), respectively. Periodic boundary conditions are applied to all three directions. The energy of the system is minimized using the conjugate gradient method with 50,000-time steps. After the energy minimization, the system is equilibrated in two stages: (i) about 5.5 ns in the *NPT*-ensemble, and (ii) for an additional 0.5 ns in the *NVT*-ensemble. A long equilibration run in the *NPT*-ensemble is needed because of the high pressure.

The adsorption of viscosifiers is studied by placing a single polymer in the center of the simulation box in CO_2 bulk phase (Fig. 2) then performing SMD simulations in the *NPT*-ensemble. In the SMD simulations, a virtual spring with a harmonic potential connects the pre-identified group (or atom) within the polymer and a dummy atom

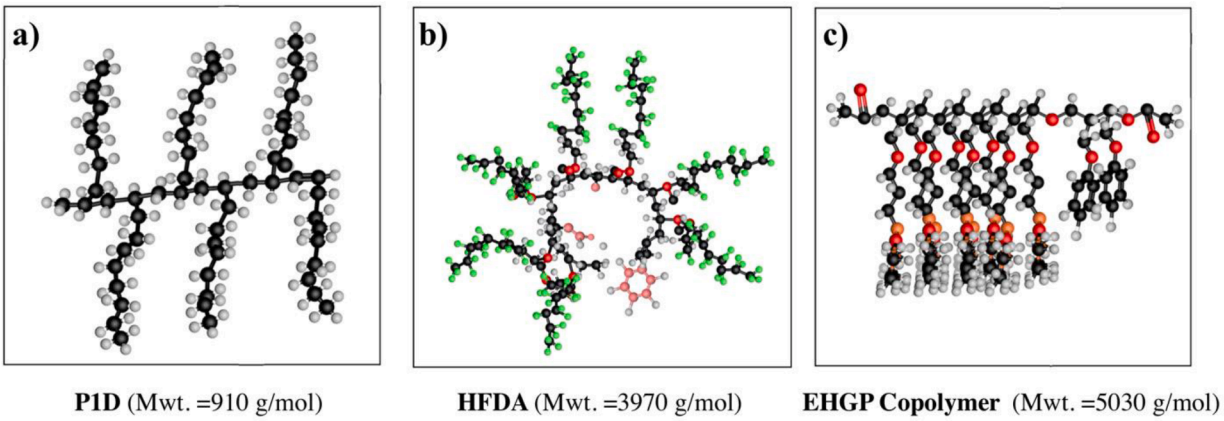

Fig. 1. Chemical structure of CO_2 viscosifiers: (a) P1D: $[CH_2CH[(CH)_2)_7CH_3]]_n$, with $n = 6$, ((b) HFDA: $C_{25}H_{40}O_2(C_9F_{19})_x(C_6H_5)_y$, with $x = 7$, $y = 3$. (c) EHGP Copolymer: $(C_{13}H_{32}O_4Si_3)_8(C_9H_{10}O_2)_2$. Color code: white; hydrogen, black, carbon; red, oxygen; orange, silicon; pink, styrene, and green, fluorine.

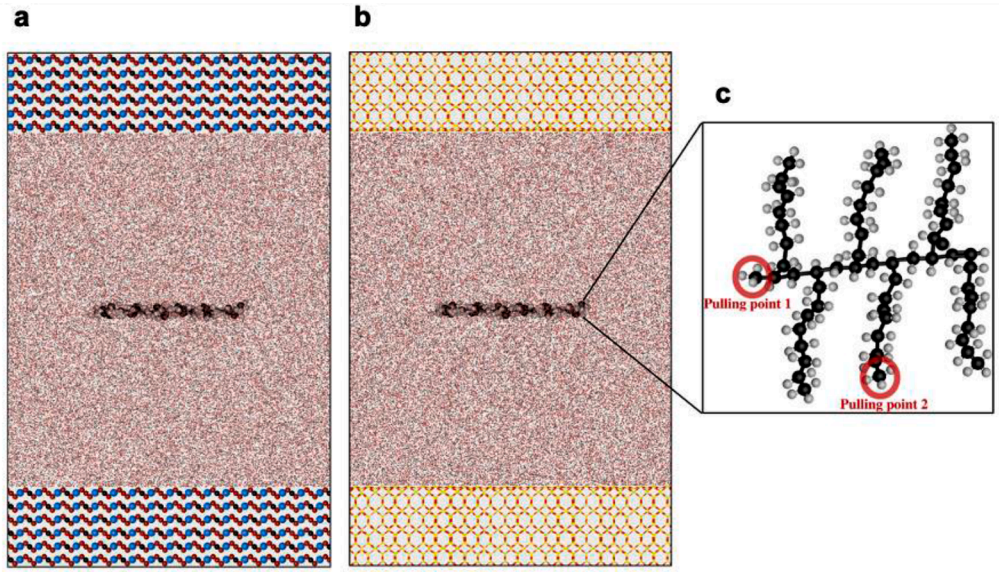

Fig. 2. Initial configuration of P1D in CO_2 phase placed 3 nm away from top and bottom surfaces of calcite slabs (a) and α-quartz slabs (b), fully immersed in the CO_2 phase. Illustration of the pulling group in PID (c). The fluid domain size is $x = y = 8.5$ nm, and z (distance between top and bottom solid surfaces) = 6 nm for all three viscosifier molecules.

using tether style command in LAMMPS. In this work, pulling procedures with minor differences are applied to investigate different molecules with different structures. For example, P1D is pulled toward the rock surfaces twice and an averaged pulling is recorded (see Fig. 3).

For HFDA and EHGP co-polymer, the pulling is applied only once to the molecule's center of mass. In all polymers, the dummy atom is moved very slowly at a constant velocity v along the z-direction using **cvel** mode command in LAMMPS. The potential of the harmonic spring is defined as

$$U_{spring} = \frac{1}{2}\, k\, \left[vt - \left(z_f - z_o\right)\right]^2 \tag{1}$$

where k is the spring constant, v is the pulling velocity, t is time, and z_f and z_o are the current and initial positions of the pre-identified group in the polymer, respectively. The values of k and v are set to 2000 kJ/mol. nm^2 and 3×10^{-3} Å/ps, respectively. These values are partly based on quasi-equilibrium considerations. The work done to pull the polymer toward the surface can be expressed as

$$W = \int_{z_o}^{zf} \Delta U_{spring}.dz' \tag{2}$$

where z_f is the final position of the pre-identified group or atom in the polymer. The change in Gibbs free energy (ΔG) (also called potential of mean force (PMF)) can be calculated using the Jarzynski equality (Park et al., 2003) i.e.,

$$\Delta G = -W \tag{3}$$

Provided the pulling is slow, the process is quasi-equilibrium. In general, the difference between ΔG and $-W$ is dissipation.

4. Results

4.1. Molecular simulations

The essence of steered molecular dynamics simulation is presented in Fig. 3 where the PMF is plotted vs distance from the surface of calcite and α-quartz. A negative PMF indicates adsorption. A relatively large

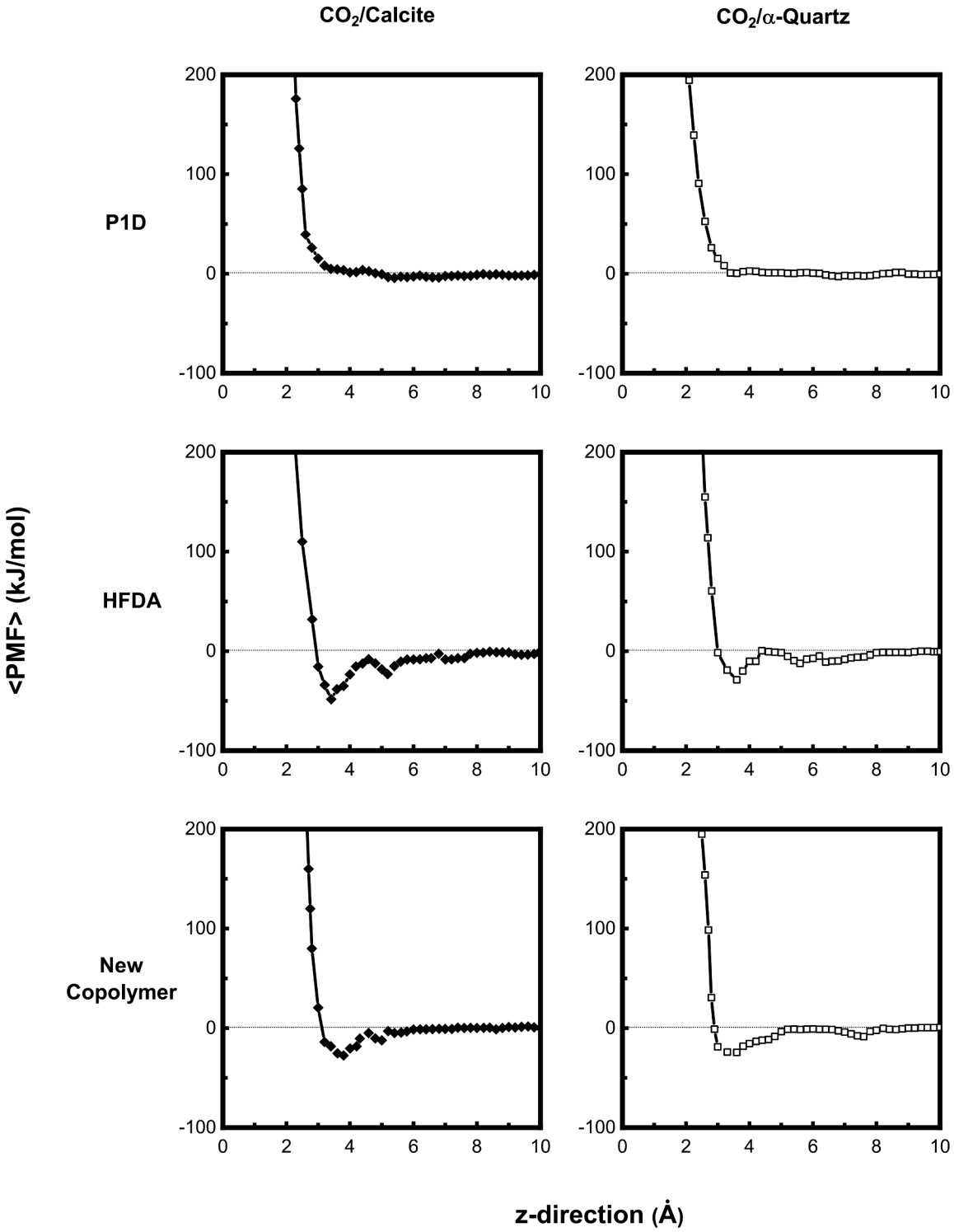

Fig. 3. Potential of mean force (PMF) vs. the distance from the surface of calcite (first column) and α-quartz (second column): P1D (firs row), HFDA (second row), and the EHGP co-polymer (third row designated as the New Co-polymer)). $P = 7700$ psi and $T = 185$ F.

negative value of PMF implies strong adsorption. Panels on the first row in Fig. 3 give a clear indication that P1D molecule does not show a tendency for adsorption onto the calcite and α-quartz surfaces. The fluorinated molecule HFDA and the EHGP co-polymer both show strong tendency for adsorption (panels in the second and third rows in Fig. 3).

4.2. Viscosification by P1D (average molecular weight =2950 g/mol)

Fig. 4 shows the measured relative viscosity for the mixture of 1.5 wt % P1D of 2950 molecular weight (g/mol) and supercritical CO_2. The viscosity of neat CO_2 serves as the reference, in the temperature range of 95 to 194 F at the pressure of 3500 psi. The temperature is increased step by step, and two readings are made at each target temperature. Afterward, the temperature is decreased from 194 to 95 F, and two readings

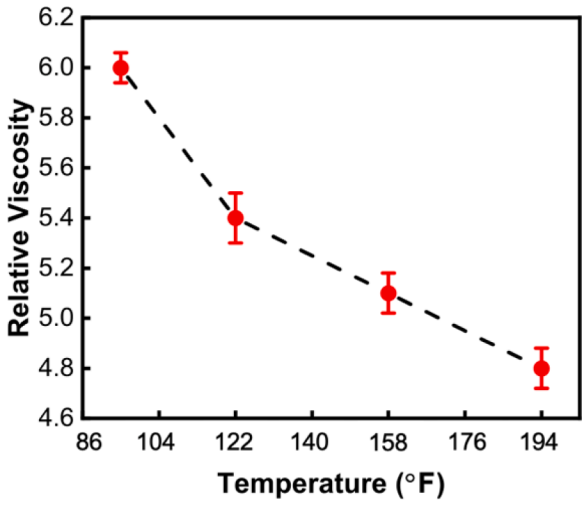

Fig. 4. Relative viscosity vs. temperature for 1.5 wt% P1D (average molecular weight= 2950 g/mol) and CO_2 mixture in the temperature range of 95 to 194 ℉ and at P = 3500 psi. The error bars show the variation of readings at each temperature.

are made again at each temperature. The error bars in Fig. 4 show the variation of the readings at each temperature. The results also indicate that P1D is stable over the temperature range, i.e., the same relative viscosity values are obtained after the mixture is exposed to temperature increase and decrease. The solubility and viscosification of various oligomers of 1-decene are presented in Ref. Kar and Firoozabadi (2022). The remarkable results from the P1D with an average molecular weight of about 2950 is due to two different features of the molecule. The high number of methyl groups which results in high solubility in CO_2 and branching which affects viscosification (Kar and Firoozabadi, 2022; Kobayashi and Firoozabadi, 2022)

4.3. Adsorption evaluation of P1D in sandstone rock

The first set of core flooding experiments are conducted to evaluate adsorption of P1D in porous media. The adsorption of polymer onto the rock surface may affect flow in two ways. The adsorbed molecules may block the pores leading to a decrease in permeability. A permeability impairment can cause serious injectivity and eventually formation damage, especially near the wellbore region. Another effect of polymer adsorption on the rock surface is reduction in CO_2-phase viscosity due to lower concentration of polymer.

Fig. 5a shows pressure drops in the high permeability core sample. First, neat CO_2 is injected into the core at the injection rate of 2.5 PV/hr until pressure is stabilized at 0.14 psi. Then viscosified CO_2 is injected at the same injection rate; the injection is continued until a constant pressure drop is observed (0.64 psi). After switching to the viscosified CO_2, the pressure drop has an increasing trend for the first pore volume. During the injection of the second pore volume of viscosified CO_2, the pressure drop is stabilized at 0.64 psi. The ratio of stabilized pressure drop at the end of neat CO_2 and viscosified CO_2 injection is 4.6, comparable to the measured relative viscosity of 4.8. This is the most reliable indication that the polymer does not have appreciable adsorption to the rock surface. Direct adsorption measurements will further establish the low adsorption and quantify the amount.

The injection fluid is then switched back to neat CO_2 to examine change in permeability of the core due to polymer retention and adsorption. After injecting of almost one pore volume of neat CO_2, the pressure drop stabilizes at the value of 0.16 psi. The slight difference between pressure drops at the end of two neat CO_2 injection periods might be due to low adsorption/retention of polymer on the rock surface. To further confirm this hypothesis, the neat CO_2 injection is continued at a higher rate (5 PV/hr) for two more pore volumes, and then the rate is switched back to 2.5 PV/hr until approaching stabilized pressure drop (0.15 psi). The minor reduction in the stabilized pressure drop may confirm negligible adsorption of the polymer on the surface of the rock sample. The investigation of very low adsorption will be further pursued in this work when pressure drop is significantly higher than the accuracy limit of the pressure transducer (0.14 psi).

To examine the effects of core permeability on adsorption of viscosified CO_2, the second evaluation of adsorption is conducted in a core with intermediate permeability. Fig. 5b shows pressure drop across a core with intermediate permeability. The pressure drop in neat CO_2 injection is stabilized at 0.21 psi. The same trend is observed as the high permeable core. The pressure drop starts to increase upon switching to viscosified CO_2 during the first injection pore volume and then stabilizes at 0.93 psi. The ratio of the pressure drops for the neat and viscosified CO_2 is 4.4 which is in agreement with the relative viscosity value of 4.8. Switching back to neat CO_2 leads to a decreasing trend in the pressure drop, and it eventually stabilizes at 0.24 psi which is slightly higher than the primary pressure drop of 0.21 psi in neat CO_2. Comparing the relative viscosity and the stabilized pressure drop ratio for neat and viscosified CO_2 indicates an 8% difference that may be due to low adsorption of the polymer onto the rock surface.

To verify our mixing and adsorption evaluation procedure, the commercial P1D with 6 repeat units is investigated for pressure drop in flow; the results are shown in Fig. 5c. The measured relative viscosity at the concentration of 2 wt%, pressure of 3500 psi, and temperature of 194 ℉ is 1.8 from Kar and Firoozabadi (2022), as well as our measurements using the setup described above. We perform flow testing from injection of the viscosified CO_2 and comparison with neat CO_2 flow in the same manner as the flow of P1D (average Mwt= 2950 g/mol) with higher molecular weight in high and intermediate permeable cores. The stabilized pressure drop for the neat CO_2 injection is 0.8 psi, and upon switching to the viscosified CO_2, the pressure drop increases and stabilizes at 1.26 psi after the first pore volume injection. There have been large variations in the reported viscosification of P1D with 6 repeat units in the literature (Heller et al., 1985; Zhang et al., 2011; Al Hinai et al., 2017). The large disparity in the measured relative viscosity may be due to use of inefficient mixing techniques, and viscosity measurement methods. At 2 wt% concentration, the agreement between viscosity measurements (relative viscosity of 1.8) and the ratio of pressure drops during neat and viscosified CO_2 injection (1.6) in Test 3 demonstrate the accuracy of both mixing and viscosity measurement setups in our work.

4.4. Brine displacement

4.4.1. High permeability media: short core

We evaluate the efficiency of the P1D in improving sweep efficiency in CO_2 injection in the brine-saturated sandstone. In the experimental design, three main parameters are determined in both neat and viscosified CO_2 injection: (1) breakthrough time, (2) brine production, and (3) pressure drop across the core. Due to low pressure drop in the high permeability core below the accuracy of the pressure transducer, only results for medium permeability short cores and high permeability long cores are presented. The data are provided in the Supporting Information. The breakthrough time is a good measure of mobility control and sweep efficiency. Fig. 6a shows brine displacement by neat and by viscosified CO_2 at injection rate of 0.26 PV/hr. The breakthrough occurs at injection of 0.24 and 0.62 PV for neat and viscosified CO_2, respectively. The brine production increases from 36% for the neat CO_2 to 68% PV for the viscosified CO_2. In viscosified injection, a major amount of the produced brine is before the breakthrough, and the production starts to smoothen after breakthrough. The results reveal a significant delay in breakthrough time and an increase in brine production from CO_2 viscosification.

To investigate the effect of injection rate on brine production and breakthrough time, the brine displacement experiments are repeated at

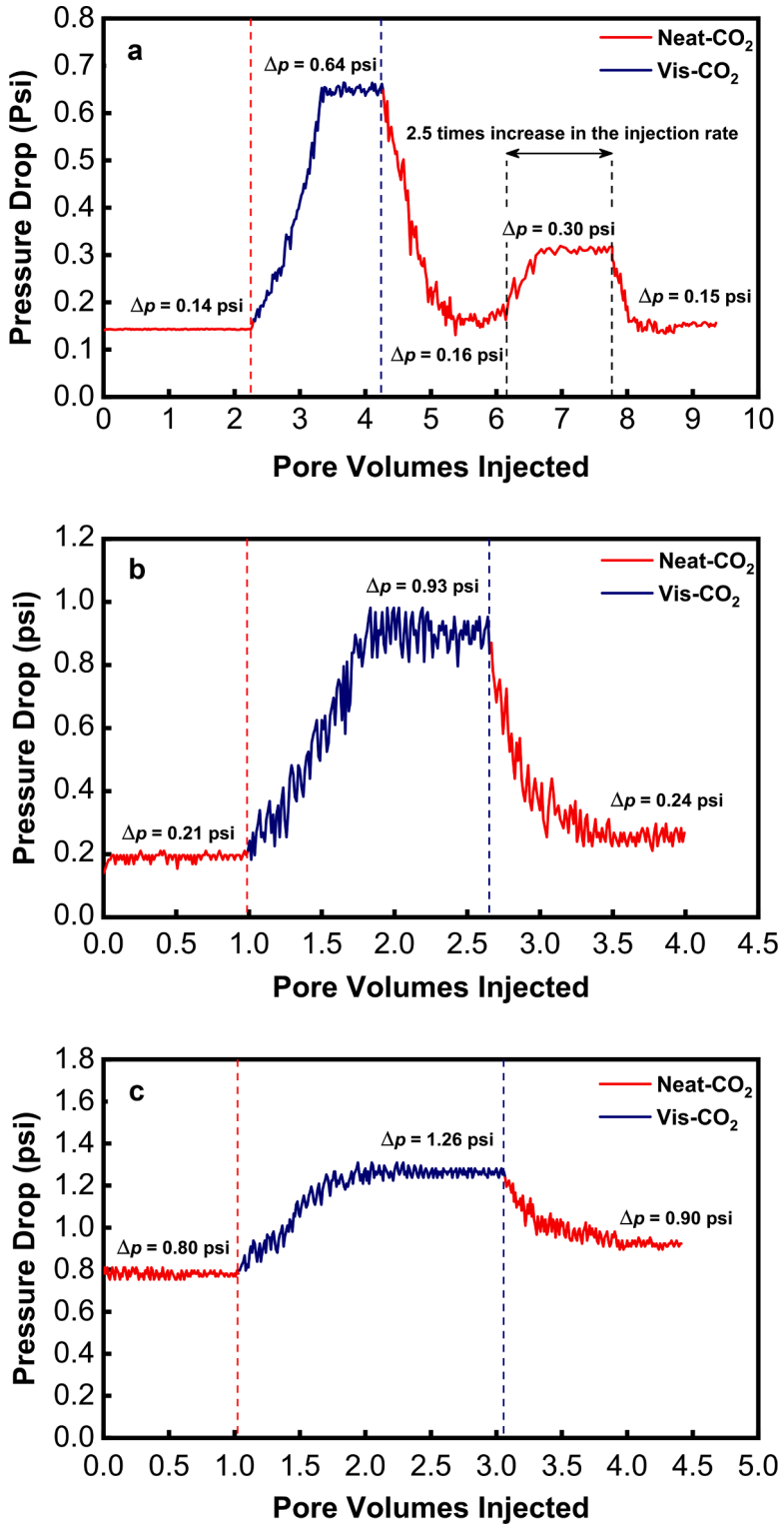

Fig. 5. Pressure drop vs. PVI in (a) Test 1; high permeability sandstone core with P1D (average Mwt=2950 g/mol), (b) Test 2; intermediate permeability sandstone core (97 mD) with P1D (average Mwt = 2950 g/mol), and (c) Test 3; ntermediate permeability sandstone cores with P1D (average Mwt= 910 g/mol). Injection rate 2.5 PV/hr. $T = 194$ °F. Outlet $P = 3500$ psi. Horizontal core orientation.

a higher injection rate of 1 PV/hr. The results in Fig. 6a show that the increased injection rate has no significant effects on the overall trend of brine production. The breakthrough time for the neat CO_2 is slightly lower at the higher injection rate, 0.22 PV compared to 0.24 PV. The brine production is slightly higher when the injection rate is increased to 1 PV/hr. The improvement in breakthrough time and brine production can be observed in viscosified CO_2.

4.4.2. *Intermediate permeability media: short core*

The effect of permeability on brine displacement efficiency is also investigated in viscosified CO_2 injection. Fig. 6b depicts brine production in injection of neat and viscosified CO_2 in cores of intermediate

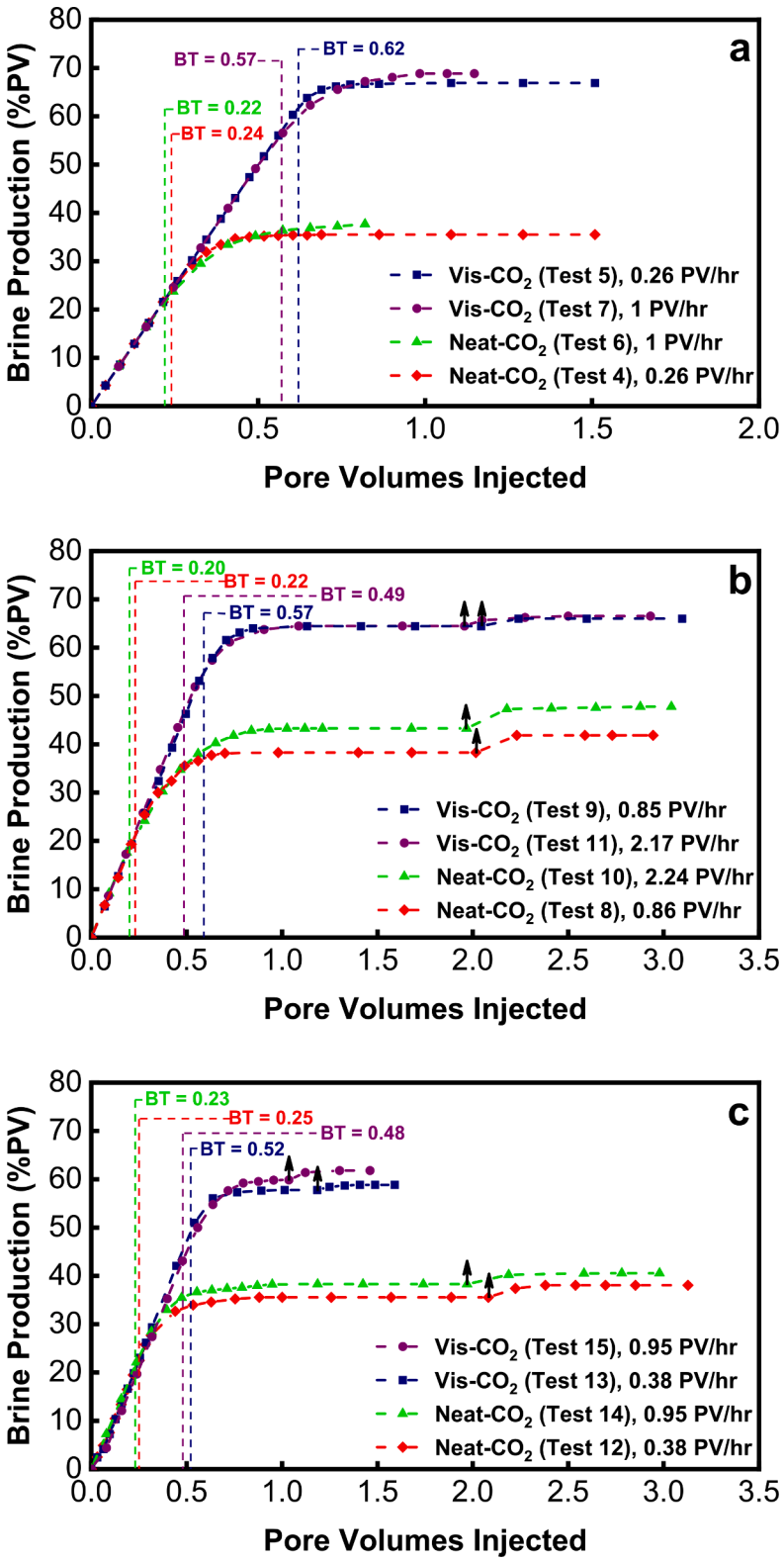

Fig. 6. Brine production vs. PVI in (a) High permeability short sandstone cores: Neat CO_2 (Tests 4 and 6) and viscosified CO_2 (Tests 5 and 7); (b) Intermediate permeability short sandstone cores: Neat CO_2 (Tests 8 and 10) and viscosified CO_2 (Tests 9 and 11); (c) High permeability long sandstone cores: Neat CO_2 (Test 12 and 14) and viscosified CO_2 (Tests 13 and 15). $T = 194$ ℉ (except for Tests 6 and 7, $T = 158$ ℉). Outlet $P = 3500$ psi. Horizontal core orientation. The symbol "↑" indicates the time (in terms of PV) that the injection rate is increased by 2.5 times.

permeability at injection rates of 0.85 and 2.24 PV/hr. There is a significant delayed breakthrough time in viscosified CO_2 injections at both injection rates. In viscosified CO_2 injection at the rate of 0.85 PV/hr, the breakthrough is at 0.57 PVI, which is 2.6 times higher than the breakthrough time in the neat CO_2 experiment at comparable injection rate. At the higher injection rate, the breakthrough time is delayed from 0.20 PVI in neat CO_2 to 0.49 PVI in viscosified CO_2.

The results above demonstrate a significant effect of viscosification on brine production increase, i.e., from 0.42 to 0.66 at the low injection rate and from 0.48 to 0.67 at the high injection rate. In each drainage experiment, the injection rate is increased 2.5 times after 2 PV injection. We observe that in neat CO_2, the brine production increases 4–5% after the rate increase. In viscosified CO_2, the brine production increase is 2%. The difference may be attributed to gravity segregation and/or the

capillary end effect. Long core experiments to be presented next will help to examine the end effect further. The pressure drop data in the injection of neat and viscosified CO_2 are presented in Fig. S2a for the intermediate permeable cores.

4.4.3. High permeability media: long core

In a long core, the contribution of capillary end effect to the production of brine is less than in a short core. As a result, the contribution of gravity segregation may be better known. The injection rate is kept the same as in the short core; the injection rates in terms of PV are 0.38 and 0.95 PV/hr. The brine production data are presented in Fig. 6c. The delayed breakthrough time has a similar trend as in the short cores. Therefore, the capillary end effect may not be significant in the shorter cores. The pressure drop data are shown in Fig. S2b.

4.4.4. Vertical short cores

The effect of CO_2 viscosification on residual brine saturation is evaluated in vertical core experiments. Fig. 7 shows brine production in the vertical experiments. Three main differences can be observed compared to the horizontal experiments. First, the breakthrough time for both neat and viscosified CO_2 (0.61 and 0.75 PVI) is higher than the corresponding values in the horizontal core flow (0.22 and 0.57 PVI). Second, the brine production at the end of the vertical core experiments is significantly higher than the corresponding horizontal cores. The extra brine production due to the increase in the injection rate at the end of the experiments are significantly lower in vertical tests. The pressure drop plots of the vertical experiments depicted in Fig. S3 indicate the same characteristics observed in the horizontal core plots. We estimate the residual brine saturation to be 40% in neat CO_2 and 27% in viscosified CO_2. There is a major effect of viscosification in reduction of residual brine saturation. We are currently investigating the mechanism that leads to reduction of residual brine saturation despite very low adsorption. Preliminary molecular simulations show that there is no significant effect of the P1D in the interfacial tension of the brine-CO_2. Preliminary molecular simulations also reveal that the polymer does not have an appreciable effect on contact angle in the CO_2-brine-quartz system. These results are in line with very low adsorption of the P1D in core flooding experiments. In a recent work, (Kar et al., 2022) have demonstrated that the residual oil saturation from brine displacement correlates with interfacial elasticity but not with contact angle. For the CO_2-brine-chemical system, (Barrabino et al., 2021) have measured interfacial elasticity parameters G' and G''. Based on these measurements we have calculated the phase angle; it varies in the range of 20 to 40°. The phase angles indicate that the interface has become elastic due to the chemical. The interfacial elasticity from the work of Barrabino et al.(Barrabino et al., 2021) agrees with residual brine saturations by Føyen et al. (2020) which we discussed in the introduction. It is likely that the interfacial elasticity may have the same effect in residual oil saturations and in residual brine saturation.

The main objective of CO_2 viscosification is to improve mobility control and sweep efficiency of the CO_2 phase. The significant delay in CO_2 breakthrough time and increase of brine production in viscosification by the P1D molecule (with about twenty repeat units) in horizontal core flooding experiments demonstrate the improved sweep efficiency. The difference between water saturations at CO_2 breakthrough and end of the injection, which is another criterion for evaluating displacement efficiency, is much lower in viscosified CO_2 than neat CO_2. The P1D molecule also reduces the residual brine saturation in drainage. The combination of mobility control and residual brine saturation reduction results in a delayed breakthrough time of 2.4 folds in various horizontal coreflood experiments. Three different salt compositions in the concentration range of 50 to 73 mg/L are used in core flooding with the P1D molecule. Unlike CO_2-foam, no significant difference is observed in performance of viscosified CO_2 from salt effect.

It should be noted that the degree of CO_2 viscosity enhancement reported in Kar and Firoozabadi (2022) is significantly greater than the degree of thickening reported for the dissolution of similar oligomers such as oligomers of 1-decene with six monomers. Typically, very high molecular weight polymers (100,000 - 10,000,000 g/gmol) have been used to significantly increase the viscosity of CO_2 (Lemaire et al., 2021a). In this work we establish that the P1D molecules do not adsorb to the rock surfaces through molecular simulations and by coreflooding experiments in sandstone. In an early paper in 1987, (Dandge and Heller, 1987) synthesized polymers of 1-hexene and did preliminary work on dissolution and viscosification of light normal alkanes. The falling cylinder time is presented as a measure of viscosifcation. The synthesized polymer consisted of various polymers. There may be significant differences between viscosification of CO_2 and non-polar hydrocarbons.

5. Conclusions

In this work, for the first time we present data and measurements on efficient displacement of brine by viscosifying CO_2 in sandstone rocks. The work is in relation to mitigation of climate change through directing its storage in the subsurface with efficiency. A state-of-art setup is designed to thoroughly mix CO_2 with viscosifying polymer P1D with an average molecular weight of 2950 g/mol at the desired concentration,

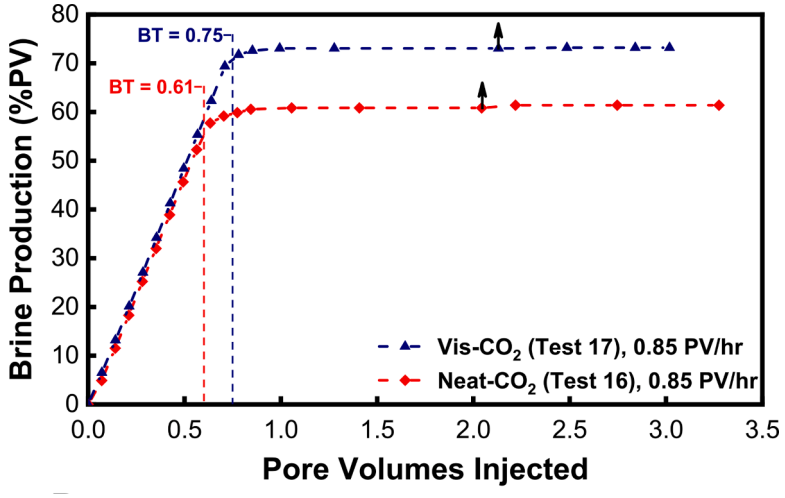

Fig. 7. Brine production vs. PVI for intermediate permeability short sandstone cores in vertical direction. Neat CO_2 (Tests 16) and viscosified CO_2 (Tests 17). $T = 194$ F. outlet $P = 3500$ psi. The symbol "↑" indicates the time (in terms of PV) that the injection rate is increased by 2.5 times.

pressure, and temperature. The viscosified CO_2 is injected into high and intermediate permeability sandstone cores to evaluate adsorption, breakthrough, and brine production. The residual brine saturation is measured for both neat and viscosified drainage displacement. Major conclusions from our work are:

1. Mixing 1.5 wt% of P1D (average molecular weight = 2950 g/mole) with CO_2 at pressure of 3500 psi and temperature of 95 ℉ increases the viscosity of CO_2 six folds. The relative viscosity decreases mildly upon increasing the temperature; it is 4.8 times at pressure of 3500 psi and temperature of 194 ℉. Our measurements show that the relative viscosity in the cooling process from 194 to 95 ℉, in rigorous mixing at 1500 rpm is reversible at high pressure conditions.
2. The ratio of stabilized pressure drop for the neat and viscosified CO_2 injection core flooding experiments is close to the relative viscosity of viscosified CO_2. A major conclusion is that the adsorption is small. The core flooding results provides a clear demonstration of effectiveness of the molecule used in our work.
3. The brine displacement experiments in the cores with high and intermediate permeability indicate that viscosifying CO_2 leads to delay in the gas breakthrough with an average of 2.4 times and an increase in the brine production with an average of aboutv1.6 times. No significant differences can be detected between long and short cores in effectiveness of the P1D on delaying the breakthrough and increase of brine production.
4. The performance of the molecule is not affected by salt composition and salt concentration in the aqueous phase.
5. The oligomer of 1-decene with about twenty repeat units not only is very effective in CO_2 viscosification, but also reduces the residual water saturation from 40 to about 27% at 3500 psi and 194 ℉. The combination may result in significant increase in efficiency of CO_2 storage.

Declarations

The authors, Salar Afra, Mohamed Alhosani and abbas firoozabadi have no conflict of interest in relation to this work.

CRediT authorship contribution statement

Salar Afra: Conceptualization, Investigation, Writing – review & editing. **Mohamed Alhosani:** Conceptualization, Methodology, Writing – review & editing. **Abbas Firoozabadi:** Conceptualization, Supervision, Writing – review & editing, Funding acquisition.

Declaration of Competing Interest

The authors declare that they have no known competing financial interests or personal relationships that could have appeared to influence the work reported in this paper.

Data availability

Data will be made available on request.

Acknowledgements

We thank Equinor for the support of the work. Mohamed Alhosani was supported by Abu Dhabi National Oil Company (ADNOC).

Supplementary materials

Supplementary material associated with this article can be found, in the online version, at doi:10.1016/j.ijggc.2023.103888.

References

Letcher, T.M., 2021. Global warming—a complex situation. Clim. Change 3–17. https://doi.org/10.1016/b978-0-12-821575-3.00001-3.

Aminu, M.D., Nabavi, S.A., Rochelle, C.A., Manovic, V., 2017. A review of developments in carbon dioxide storage. Appl. Energy 208, 1389–1419. https://doi.org/10.1016/j.apenergy.2017.09.015.

Mukherjee, M., Misra, S., 2018. A review of experimental research on Enhanced Coal Bed Methane (ECBM) recovery via CO_2 sequestration. Earth Sci. Rev. 179, 392–410. https://doi.org/10.1016/j.earscirev.2018.02.018.

Kolster, C., Masnadi, M.S., Krevor, S., Mac Dowell, N., Brandt, A.R, 2017. CO_2 enhanced oil recovery: a catalyst for gigatonne-scale carbon capture and storage deployment? Energy Environ. Sci. 10, 2594–2608. https://doi.org/10.1039/c7ee02102j.

Kim, Y., Jang, H., Kim, J., Lee, J., 2017. Prediction of storage efficiency on CO_2 sequestration in deep saline aquifers using artificial neural network. Appl. Energy 185, 916–928. https://doi.org/10.1016/j.apenergy.2016.10.012.

Tayari, F., Blumsack, S., 2020. A real options approach to production and injection timing under uncertainty for CO_2 sequestration in depleted shale gas reservoirs. Appl. Energy 263, 114491. https://doi.org/10.1016/j.apenergy.2020.114491.

Iglauer, S., AZarzor, Al-, Reza, R., Maxim, L., 2015. CO_2 wettability of caprocks: implications for structuralstorage capacity and containment security. Geophys. Res. Lett. 42, 9279–9284. https://doi.org/10.1002/2015GL065787.Received.

MacMinn, C.W., Szulczewski, M.L., Juanes, R., 2010. CO_2 migration in saline aquifers. Part 1. Capillary trapping under slope and groundwater flow. J. Fluid Mech. 662, 329–351. https://doi.org/10.1017/S0022112010003319.

Pentland, C.H., El-Maghraby, R., Iglauer, S., Blunt, M.J., 2011. Measurements of the capillary trapping of super-critical carbon dioxide in Berea sandstone. Geophys. Res. Lett. 38, 2007–2010. https://doi.org/10.1029/2011GL046683.

Mutoru, J.W., Leahy-Dios, A., Firoozabadi, A., 2011. Modeling infinite dilution and Fickian diffusion coefficients of carbon dioxide in water. AlChE J. 57, 1617–1627. https://doi.org/10.1002/aic.12361.

Ennis-King, J., Preston, I., Paterson, L., 2005. Onset of convection in anisotropic porous media subject to a rapid change in boundary conditions. Phys. Fluids 17, 1–15. https://doi.org/10.1063/1.2033911.

Gershenzon, N.I., Soltanian, M., Ritzi, R.W., Dominic, D.F., 2014. Influence of small scale heterogeneity on CO_2 trapping processes in deep saline aquifers. Energy Procedia 59, 166–173. https://doi.org/10.1016/j.egypro.2014.10.363.

Heller, J.P., Dandge, D.K., Card, R.J., Donaruma, L.G., 1985. Direct thickeners for mobility control of CO_2 floods. Soc. Pet. Eng. J. 25, 679–686. https://doi.org/10.2118/11789-PA.

Føyen, T., Brattekås, B., Fernø, M.A., Barrabino, A., Holt, T., 2020. Increased CO_2 storage capacity using CO_2-foam. Int. J. Greenhouse Gas Control 96, 103016. https://doi.org/10.1016/j.ijggc.2020.103016.

Alcorn, Z.P., Føyen, T., Gauteplass, J., Benali, B., Soyke, A., Fernø, M., 2020. Pore-and core-scale insights of nanoparticle-stabilized foam for CO_2-enhanced oil recovery. Nanomaterials 10, 1–15. https://doi.org/10.3390/nano10101917.

Adebayo, A.R., 2018. Viability of foam to enhance capillary trapping of CO_2 in saline aquifers—an experimental investigation. Int. J. Greenhouse Gas Control 78, 117–124. https://doi.org/10.1016/j.ijggc.2018.08.003.

Lemaire, P.C., Alenzi, A., Lee, J.J., Beckman, E.J., Enick, R.M., 2021a. Thickening CO_2 with direct thickeners, CO_2 -in-oil emulsions, or nanoparticle dispersions: literature review and experimental validation. Energy Fuels 35, 8510–8540. https://doi.org/10.1021/acs.energyfuels.1c00314.

Enick, R.M., Olsen, D., Ammer, J., Schuller, W., 2012. Mobility and conformance control for CO_2 EOR via thickeners, foams, and gels - A literature review of 40 years of research and pilot tests. SPE - DOE Improv. Oil Recovery Symp. Proc. 2, 910–921. https://doi.org/10.2118/154122-ms.

Goicochea, A.G., Firoozabadi, A., 2019. CO_2 viscosification by functional molecules from mesoscale simulations. J. Phys. Chem. C 123, 29461–29467. https://doi.org/10.1021/acs.jpcc.9b08589.

Sun, Y., Li, Q., Yang, D., Liu, X., 2016. Laboratory core flooding experimental systems for CO_2 geosequestration: an updated review over the past decade. J. Rock Mech. Geotech. Eng. 8, 113–126. https://doi.org/10.1016/j.jrmge.2015.12.001.

Kumar, A., Noh, M., Pope, G.A., Sepehrnoori, K., Bryant, S., Lake, L.W., 2004. Reservoir simulation of CO_2 storage in deep saline aquifers. SPE - DOE Improved Oil Recovery Symp. Proc. https://doi.org/10.2118/89343-ms.

Barrabino, A, Holt, T, Kvik, B, Lindberg, E, 2021. First Approach to Measure Interfacial Rheology at High-Pressure Conditions by the Oscillating Drop Technique. Colloids Interfaces 5 (2), 23. https://doi.org/10.3390/colloids5020023.

Celia, M.A., Bachu, S., Nordbotten, J.M., Bandilla, K.W., 2015. Status of CO_2 storage in deep saline aquifers with emphasis on modeling approaches and practical simulations. Water Resour. Res. 51, 6846–6892. https://doi.org/10.1002/2015WR017609.

Müller, N., 2011. Supercritical CO_2-brine relative permeability experiments in reservoir rocks-literature review and recommendations. Transp. Porous Media 87, 367–383. https://doi.org/10.1007/s11242-010-9689-2.

Mathias, S.A., Gluyas, J.G., González Martínez de Miguel, G.J., Bryant, S.L., Wilson, D., 2013. On relative permeability data uncertainty and CO_2 injectivity estimation for brine aquifers. Int. J. Greenhouse Gas Control 12, 200–212. https://doi.org/10.1016/j.ijggc.2012.09.017.

Zaberi, H.A., Lee, J.J., Enick, R.M., Beckman, E.J., Cummings, S.D., Dailey, C., et al., 2020. An experimental feasibility study on the use of CO_2-soluble polyfluoroacrylates for CO_2 mobility and conformance control applications. J. Pet. Sci. Eng. 184, 106556 https://doi.org/10.1016/j.petrol.2019.106556.

Zhang, S., She, Y., Gu, Y., 2011. Evaluation of polymers as direct thickeners for CO_2 enhanced oil recovery. J. Chem. Eng. Data 56, 1069–1079. https://doi.org/10.1021/je1010449.

Al Hinai, N.M., Saeedi, A., Wood, C.D., Valdez, R., Esteban, L., 2017. Experimental study of miscible thickened natural gas injection for enhanced oil recovery. Energy Fuels 31, 4951–4965. https://doi.org/10.1021/acs.energyfuels.7b00314.

Kar, T, Cho, H, Firoozabadi, A, 2022. Assessment of low salinity waterflooding in carbonate cores: Interfacial viscoelasticity and tuning process efficiency by use of non-ionic surfactant. J. Colloid Interface Sci. 125–133.

Kar, T., Firoozabadi, A., 2022. Effective viscosification of supercritical carbon dioxide by oligomers of 1-decene. IScience 25, 104266. https://doi.org/10.1016/j.isci.2022.104266.

Zhang, Y., Zhu, Z., Tang, J., 2021. Investigation on modified polyether as an efficient CO_2thickener. New J. Chem. 45, 651–656. https://doi.org/10.1039/d0nj02442b.

Huang, Z., Shi, C., Xu, J., Kilic, S., Enick, R.M., Beckman, E.J., 2000. Enhancement of the viscosity of carbon dioxide using styrène/fluoroacrylate copolymers. Macromolecules 33, 5437–5442. https://doi.org/10.1021/ma992043+.

Jiménez-Ángeles, F., Firoozabadi, A., 2018. Hydrophobic hydration and the effect of NaCl salt in the adsorption of hydrocarbons and surfactants on clathrate hydrates. ACS Cent. Sci. 4, 820–831. https://doi.org/10.1021/acscentsci.8b00076.

Titiloye, J.O., De Leeuw, N.H., Parker, S.C., 1998. Atomistic simulation of the differences between calcite and dolomite surfaces. Geochim. Cosmochim. Acta 62, 2637–2641. https://doi.org/10.1016/S0016-7037(98)00177-X.

France-Lanord, A., Rigby, D., Mavromaras, A., Eyert, V., Saxe, P., Freeman, C., et al., 2014. MedeA®: atomistic simulations for designing and testing materials for micro/nano electronics systems. In: Proceedings of the 15th International Conference on Thermal, Mechanical and Mulit-Physics Simulation and Experiments in Microelectronics and Microsystems (EuroSimE), pp. 1–8. https://doi.org/10.1109/EuroSimE.2014.6813850.

De Leeuw, N.H., Parker, S.C., 1998. Surface structure and morphology of calcium carbonate polymorphs calcite, aragonite, and vaterite: an atomistic approach. J. Phys. Chem. B 102, 2914–2922. https://doi.org/10.1021/jp973210f.

De Leeuw, N.H., 2002. Surface structures, stabilities, and growth of magnesian calcites: a computational investigation from the perspective of dolomite formation. Am. Mineral. 87, 679–689. https://doi.org/10.2138/am-2002-5-610.

Koleini, M.M., Badizad, M.H., Kargozarfard, Z., Ayatollahi, S., 2019. Interactions between Rock/Brine and Oil/Brine interfaces within thin brine film wetting carbonates: a molecular dynamics simulation study. Energy Fuels 33, 7983–7992. https://doi.org/10.1021/acs.energyfuels.9b00496.

Sedghi, M., Piri, M., Goual, L., 2016. Atomistic molecular dynamics simulations of crude oil/brine displacement in calcite mesopores. Langmuir 32, 3375–3384. https://doi.org/10.1021/acs.langmuir.5b04713.

Wright, L.B., Walsh, T.R., 2012. Facet selectivity of binding on quartz surfaces: free energy calculations of amino-acid analogue adsorption. J. Phys. Chem. C 116, 2933–2945. https://doi.org/10.1021/jp209554g.

Wu, G., He, L., Chen, D., 2013. Sorption and distribution of asphaltene, resin, aromatic and saturate fractions of heavy crude oil on quartz surface: molecular dynamic simulation. Chemosphere 92, 1465–1471. https://doi.org/10.1016/j.chemosphere.2013.03.057.

Gama Goicochea, A., Firoozabadi, A., 2019. Atomistic and mesoscopic simulations of the structure of CO_2 with Fluorinated and nonfluorinated copolymers. J. Phys. Chem. C 123, 17010–17018. https://doi.org/10.1021/acs.jpcc.9b04293.

Plimpton, S., 1995. Fast parallel algorithms for short-range molecular dynamics. J. Comput. Phys. 117, 1–19. https://doi.org/10.1006/jcph.1995.1039.

Yiannourakou, M., Ungerer, P., Leblanc, B., Rozanska, X., Saxe, P., Vidal-Gilbert, S., et al., 2013. Molecular simulation of adsorption in microporous materials. Oil Gas Sci. Technol. Rev. IFP Energies Nouvelles 68, 977–994. https://doi.org/10.2516/ogst/2013134.

Ungerer, P., Collell, J., Yiannourakou, M., 2015. Molecular modeling of the volumetric and thermodynamic properties of kerogen: influence of organic type and maturity. Energy Fuels 29, 91–105. https://doi.org/10.1021/ef502154k.

Collell, J., Galliero, G., Gouth, F., Montel, F., Pujol, M., Ungerer, P., et al., 2014. Molecular simulation and modelisation of methane/ethane mixtures adsorption onto a microporous molecular model of kerogen under typical reservoir conditions. Microporous Mesoporous Mater. 197, 194–203. https://doi.org/10.1016/j.micromeso.2014.06.016.

Ungerer, P., Rigby, D., Leblanc, B., Yiannourakou, M., 2014. Sensitivity of the aggregation behaviour of asphaltenes to molecular weight and structure using molecular dynamics. Mol. Simul. 40, 115–122. https://doi.org/10.1080/08927022.2013.850499.

Eastwood, J.W., Hockney, R.W., Lawrence, D.N., 1980. P3M3DP—the three-dimensional periodic particle-particle/particle-mesh program. Comput. Phys. Commun. 19, 215–261. https://doi.org/10.1016/0010-4655(80)90052-1.

Waldman, M., Hagler, A.T., 1993. New combining rules for rare gas van der waals parameters. J. Comput. Chem. 14, 1077–1084. https://doi.org/10.1002/jcc.540140909.

Hoover, W.G., 1985. Canonical dynamics: equilibrium phase-space distributions. Phys. Rev. A 31, 1695–1697. https://doi.org/10.1103/PhysRevA.31.1695.

Hoover, W.G., 1986. Constant-pressure equations of motion. Phys. Rev. A 34, 2499–2500. https://doi.org/10.1103/PhysRevA.34.2499.

Park, S., Khalili-Araghi, F., Tajkhorshid, E., Schulten, K., 2003. Free energy calculation from steered molecular dynamics simulations using Jarzynski's equality. J. Chem. Phys. 119, 3559–3566. https://doi.org/10.1063/1.1590311.

Kobayashi, K., Firoozabadi, A., 2022. Effect of branching on mutual solubility of alkane-CO_2 systems by molecular simulations. J. Phys. Chem. B 126, 8300–8308. https://doi.org/10.1021/acs.jpcb.2c05774.

Dandge, O.K., Heller, J.P., 1987. Polymers for mobility control in CO_2 floods. In: Proceedings of the SPE International Symposium on Oilfield Chemistry. San Antonio, Texas Paper Number: SPE-16271-MS SPE 16271 doi:10.2118/16271-MS.